IVYSPRING INTERNATIONAL PUBLISHER

Theranostics

2017; 7(12): 2996-3006. doi: 10.7150/thno.18459

Research Paper

Using Multifunctional Peptide Conjugated Au Nanorods for Monitoring β-amyloid Aggregation and Chemo-Photothermal Treatment of Alzheimer's Disease

Meng Li[1, 2], Yijia Guan[1, 2], Andong Zhao[1, 2], Jinsong Ren[1] and Xiaogang Qu[1]✉

1. Laboratory of Chemical Biology, State Key Laboratory of Rare Earth Resources Utilization, Changchun Institute of Applied Chemistry, Chinese Academy of Sciences, Changchun, Jilin 130022, China;
2. University of Chinese Academy of Sciences, Beijing 100039, China.

✉ Corresponding author: Tel./Fax: +86 431 85262656 E-mail: xqu@ciac.ac.cn (X. Qu).

Received: 2016.11.23; Accepted: 2017.03.02; Published: 2017.07.22

Abstract

Development of sensitive detectors of Aβ aggregates and effective inhibitors of Aβ aggregation are of diagnostic importance and therapeutic implications for Alzheimer's disease (AD) treatment. Herein, a novel strategy has been presented by self-assembly of peptide conjugated Au nanorods (AuP) as multifunctional Aβ fibrillization detectors and inhibitors. Our design combines the unique high NIR absorption property of AuNRs with two known Aβ inhibitors, Aβ15-20 and polyoxometalates (POMs). The synthesized AuP can effectively inhibit Aβ aggregation and dissociate amyloid deposits with NIR irradiation both in buffer and in mice cerebrospinal fluid (CSF), and protect cells from Aβ-related toxicity upon NIR irradiation. In addition, with the shape and size-dependent optical properties, the nanorods can also act as effective diagnostic probes to sensitively detect the Aβ aggregates. This is the first report to integrate 3 segments, an Aβ-targeting element, a reporter and inhibitors, in one drug delivery system for AD treatment.

Key words: Polyoxometalates, Au nanorod, Photothermal treatment, Aβ inhibitors, Aβ detectors, Alzheimer's Disease.

Introduction

Misfolding, aggregation and accumulation of proteins in the brain have recently been recognized to be the common cellular and molecular mechanisms of neurodegenerative diseases including Alzheimer's disease (AD), Huntington's disease (HD), Parkinson's disease (PD), amyotrophic lateral sclerosis (ALS) and prion diseases.[1,2] Among them, AD, as the most common form of neurodegenerative disorder, accounts for 65% of all dementias.[3-5] A significant body of evidences demonstrate that accumulation of tau proteins and β-amyloid peptide (Aβ) are one of major characteristics of AD.[6] Given the central role of Aβ fibrillation in AD pathology, sensitive detection of Aβ aggregates, then effective inhibition of Aβ aggregation and destabilization of the performed Aβ fibrils are of diagnostic importance and therapeutic implications for AD treatment.

For this purpose, considerable progress has already been made in screening and designing inhibitors of Aβ aggregation and toxicity.[7-9] Among these inhibitors, peptide inhibitors containing the hydrophobic core KLVFF of Aβ have been widely reported due to their targeted inhibition effects on amyloid formation.[10-12] Although promising, the rapid degradation of the peptides in plasma, low lesions targeting efficiency and poor blood-brain barrier (BBB) permeability limit their clinical application.[13,14] Therefore, to improve inhibition

efficiency, recently, our group has successfully utilized nanomaterials as peptide carriers to realize the increasing stability of the peptides without repressing their anti-aggregation effect.[15]

With the development of nanotechnology, nanoparticles have attracted much attention for their potential applications in the area of drug and gene delivery[16-19] especially for targeting brain delivery[20-22] since that the nanoparticles ranging in size from about 10-100 nm were reported to have the ability to cross the BBB.[23,24] These insights into nanoparticle transport have provided novel opportunities to intervene in the pathology of AD. Among currently well-demonstrated nano-scaled biomaterials, gold nanorod (AuNR) is one kind of most promising and widely utilized nanomaterials owing to their biocompatibility and optical tenability.[25,26] AuNRs have shown great potential for biomedical applications, especially imaging and cancer hyperthermia.[27-30]

Herein, we employ the AuNRs as the carriers to delivery Aβ15-20 (Ac-QKLVFF-NH_2), the well-known Aβ-targeted peptide inhibitor. As we and others reported previously, local heat generation (hyperthermia) could act as an effective means to dissolve Aβ aggregates.[31-33] By controlling the effective size and the aspect ratio (ratio of length to diameter), the localized surface-plasmon-resonance (LSPR) of AuNRs can be easily tailored to the near infrared region to make the AuNRs as excellent hyperthermal agents. Upon selectively attaching to Aβ aggregates by Aβ15-20 on the surface of nanorods, the performed Aβ fibrils can be dissociated utilizing the strong NIR optical absorption ability of AuNRs to generate local heat following low-power NIR laser irradiation. Photothermal therapy treatment can not only effectively reduce the side effects on normal tissue but also enhance the selectivity to lesion location compared to traditional chemotherapies[34].

Intriguingly, apart from the easily modified surface and strong NIR optical absorption ability, AuNRs attract lots of attention for their two surface plasma absorption bands, a strong, long-wavelength band in near-infrared region and a weak, short-wavelength band around 520 nm[35-38]. The longitudinal absorption band is extremely sensitive to changes in the dielectric properties of the surroundings, including solvents, adsorbates and the interparticle distance of the AuNRs[35-38]. Through binding with Aβ1-40 aggregates, the Aβ15-20 conjugated AuNRs (AuP) can assemble, resulting in coupling the plasmon band of AuNR. Therefore, our synthetic AuP can not only act as a multifunctional agent to inhibit Aβ aggregation, effectively dissociate amyloid deposits, but also be a diagnostic reagent to sensitively detect the Aβ aggregates (Figure 1).

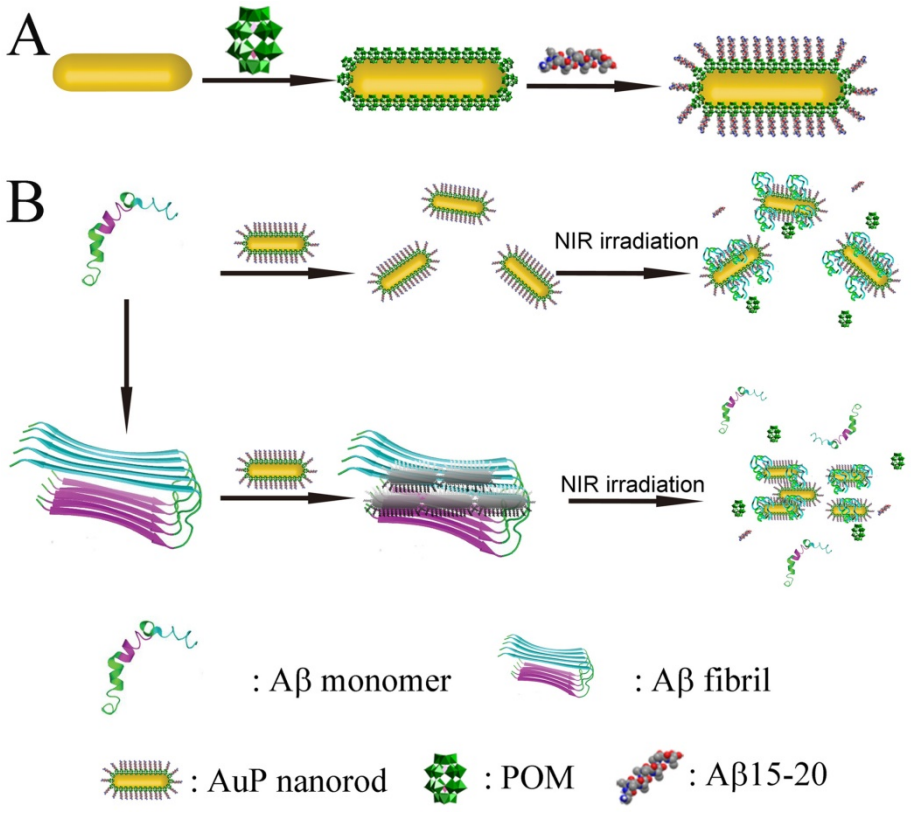

Figure 1. Schematic representation of the peptide conjugated Au nanorods used for AD treatment. (A) The schematic illustration of the preparation of AuP nanorods. (B) The peptide-conjugated Au nanorod with high NIR absorbance used for AD diagnosis and treatment.

In this work, we employ polyoxometalates (POMs) as the linkers to conjugate Aβ15-20 on the surface of AuNRs through noncovalent strategies. POMs as a class of early-transition-metal-oxygen-anion nanoclusters offer rich structural versatility and enormous applications.[39-47] Due to the negatively charged property, POMs can easily attach to the 2-aminoethanethiol coated AuNRs to obtain POM loaded AuNRs (Au-POM). According to our previous report, Aβ15-20 can easily interact with the POMs[15] to obtain the Aβ15-20 conjugated AuNRs (AuP). The noncovalent binding model is adopted to avoid the formation of self-assembled Aβ15-20 monolayers with β-sheet structure on the surface of AuNRs.[48] Furthermore, the POMs have also been demonstrated to effectively inhibit Aβ aggregation.[49] The presence of POMs in the system would enhance the anti-aggregation efficiency.

Materials and Methods

Chemicals and Instruments

Sodium borohydride ($NaBH_4$), ascorbic acid, silver nitrate ($AgNO_3$), tetrachloroauric acid ($HAuCl_4$), Thioflavin-S (ThS) and Aβ15-20 were purchased from Sigma-Aldrich. N-cetyltrimethylammonium bromide (CTAB) was obtained from Alfa Aesar. 2-aminoethanethiol was purchased from Aladdin. Aβ1-40 was obtained from American peptide. POMs were gifts from Prof. Wang. All the chemicals were used as received without further purification. Distilled water (18.2 MΩ; Millpore Co., USA) was used in all experiments and to prepare all buffers. Ultraviolet-visible spectroscopy (UV-vis) measurements were recorded on a Jasco-V550 UV-Vis spectrophotometer. To determine the composition of the as-prepared samples, in situ energy-dispersive X-ray spectroscopy (EDS) analysis were performed using a HITACHI S-4500 instrument. X-ray photoelectron spectra (XPS) were acquired on an ESCALab220i-XL electron spectrometer from VG Scientific using 300W Al Kα as the excitation source. The binding energies obtained in the XPS spectral analysis were corrected for specimen charging by referencing C1s to 284.8 eV. TEM images were recorded using a FEI TECNAI G2 20 high-resolution transmission electron microscope operating at 200 kV. The zeta potential of the nanoparticles in water was measured in a Zetasizer 3000HS analyzer.

Preparation of Au nanorods

Cetyltrimethylammonium bromide (CTAB) solution (1.0 mL, 0.20 M) was added to 1.0 mL of 0.5 mM $HAuCl_4$ and stirred. Then 0.12 mL of ice-cold 0.01 M $NaBH_4$ was dropped into the stirred solution, resulting in the formation of a brownish-yellow solution. After the seed solution was stirred continuously for 2 minutes, it was kept at 25 ^oC. The growth solution was prepared by mixing 100 mL of 0.2 M CTAB, 5.6 mL of 4 mM $AgNO_3$, 6.5 mL of 23 mM $HAuCl_4$ and 95 mL of Milli-Q water together in 250 ml flask. Ascorbic acid (0.08 M, approximately 2.5 mL) was slowly added dropwise into the reaction mixture, until the mixture became colorless after which one quarter more of the total number of droplets to that point was added. The final step was adding 1.8 mL of the seed solution to the growth solution at 27-30 ^oC. The color of the solution gradually changed within 10-20 minutes. The temperature of the growth medium was kept constant at 27-30 ^oC during the full procedure.

Preparation of Amine Modified Gold Nanorods

After preparation of CTAB-stabilized gold nanorods, excess CTAB molecules on the nanorods (10 mL solution) were removed by centrifuging once at 8000 rpm, discarding the supernatant and redispersing the particles in pure water. Then 1 mL of 30 mM 2-aminoethanethiol was added, and the solution was kept at 50 ^oC under constant sonication for 3 h. This procedure was then followed by centrifugation at 8000 rpm for 10 min to remove excess CTAB and 2-aminoethanethiol.

Preparation of POM coated Gold Nanorods

Amine modified gold nanorods (AuNR-NH_2) were dispersed in Milli-Q water (5 mL) and added 2 mM POMs (500 µL) under vigorous stirring. POMs adsorption was allowed to proceed for 6 h. This procedure was then followed by centrifugation at 8000 rpm for 10 min to remove excess POMs. The amount of POMs absorbed on the surface of Au nanorod was 38 µM / nM Au nanorods.

Preparation of peptide coated Gold Nanorods

POMs coated gold nanorods were dispersed in 5 mL pure water (3 nM) and 50 µL of a 12.8 mM Aβ15-20 /HFIP solution was added to the Au-POM solution at room temperature under vigorous stirring. Peptide adsorption was allowed to proceed for 12 h. This procedure was then followed by centrifugation at 8000 rpm for 10 min to remove excess peptide. The amount of peptides attached on the surface of Au nanorod was 32 µM / nM Au nanorods.

Aβ fibrils formation

Aβ1-40 (lot no. U10012) was purchased from American Peptide and prepared as follows. The powered Aβ1-40 peptide was first dissolved in 1,1,1,3,3,3-hexafluoropropan-2-ol (HFIP) at a

concentration of 1mg mL^{-1}. The solution was shaken at 4 °C for 2 h in a sealed vial for further dissolution and was then stored at -20 °C as a stock solution. Before use, the solvent HFIP was removed by evaporation under a gentle stream of nitrogen and the peptide was dissolved in water. Aβ1-40 self-aggregation was accomplished by mixing an aliquot of the peptides from the stock solution into aggregation buffer (10 mM Tris in 150 mM NaCl, pH 7.3) at 37 °C for 7 days.

ThT Fluorescence Measurements

The kinetics of Aβ1-40 aggregation was monitored by using ThT fluorescence assay. During the incubation, at each point of analysis (1, 2, 3, 4, 5, 6, 7 days), aggregated Aβ1-40/AuP nanorods samples were diluted to a final concentration of 2 μM (Aβ1-40 concentration) into aggregation buffer at pH 7.3 containing 10 μM ThT for fluorescence measurements. ThT is a benzothiazole dye which can selectively bind to Aβ fibrils, instead of Aβ monomers. Upon binding with β-sheet regions presented in Aβ fibrils, ThT undergoes characteristic spectral alteration, resulting in great enhancement of ThT fluorescence. When ThT is added to samples containing β-sheet-rich deposits, it fluoresces strongly with excitation and emission maxima at approximately 444 and 482 nm, respectively. The reaction is initiated immediately upon mixing β-amyloid into an aqueous environment and is completed within 1 min. Therefore, the fluorescence of ThT is dependent on the formation of amyloid fibrils. Fluorescence measurements were carried out with a JASCO FP6500 spectrofluorometer. The fluorescence signal (excitation at 444 nm) was recorded between 460 and 650 nm; 5 nm slits were used for both emission and excitation measurements. For inhibition and disaggregation experiment, the concentrations of ThT and Aβ1-40 for measurements are 10 μM and 2 μM, respectively. To obtain the proper fluorescence intensity values, fluorescence data must be corrected for the inner filter effect caused by attenuation of the excitation beam and emission signal because of the absorption by quencher and fluorophore which led to artificial decreases in the fluorescence intensities. This effect was corrected with knowledge of the absorbance values from the corresponding spectra[50,51]. The fluorescence of the system can be corrected using the following equation:

$$F_{corr} = F_{obs} \log^{-1} [(A_{ex} + A_{em}) /2]$$

where F_{corr} and F_{obs} were the corrected and observed fluorescence intensity. A_{ex} was the absorbance value at the excitation wavelength and A_{em} was the absorbance value at the emission wavelength.

Atomic Force Microscopy

For the atomic force microscopy (AFM) measurements, samples were diluted with deionized H_2O to yield a final concentration of 1 μM. Then the sample (20 μL) was applied onto freshly cleaved muscovite mica and allowed to dry. Data were acquired in the tapping mode on a Nanoscope V multimode atomic force microscope (Veeco Instruments, USA).

Inhibition of Aβ1-40 aggregation with or without NIR-irradiation

Aβ1-40 monomers was incubated with AuP nanorods in 10 mM Tris buffer (150 mM NaCl, pH 7.3) at 37 °C for 20 minutes with or without irradiation using an 808 nm NIR laser (1W/cm^2) for 8 minutes, and the mixture was further incubated at 37 °C for 7 days.

Disaggregation of Aβ1-40 fibrils with NIR irradiation

Aβ1-40 monomers was incubated in 10 mM Tris buffer (150 mM NaCl, pH 7.3) for 7 days to obtain Aβ1-40 fibrils, then a solution of AuP was added. The mixture was incubated at 37 °C for 20 minutes. Afterward, the mixture was irradiated using an 808 nm NIR laser (1W/cm^2) for 8 minutes.

Cell Toxicity Assays

PC12 cells (rat pheochromocytoma, American Type Culture Collection) were cultured in Iscove modified Dulbecco medium (IMDM, Gibco BRL) supplemented with 5% fetal bovine serum and 10% horse serum in a humidified 5% CO_2 environment at 37 °C. Cells were plated at a density of 10000 cells per well on 96-well plates in fresh medium. After 24 h, Aβ1-40 peptides (5 μM) that had been aged with or without AuP were added, and the cells were further incubated for 48 h at 37 °C. Cytotoxicity was measured by using a modified MTT assay kit (Promega). Absorbance values of formazan were determined at 570 nm with an automatic plate reader.

Animal Experiments

Animal care and handing procedures were according to the guidelines of the Regional Ethics Committee for Animal Experiments. S4880202 normal mice which were purchased from the Laboratory Animal Center of Jilin University (Changchun, China) were chosen as test animals, in a weight range of 20-25 g (8-12 weeks old) and random in sex. Cerebrospinal fluid (CSF) was collected under anesthesia using a glass pulled micropipette after exposure of the cisterna magna, taking care not to contaminate the CSF with blood. Two to 10 μL was routinely collected.

The CSF was immediately diluted 1:10 in 1% 3-[(3-cholamidopropyl)-dimethyl-ammonio]-1-propa ne sulfonate (CHAPS) in phosphate buffered saline (PBS) with protease inhibitors (Roche Diagnostics, Mannheim, Germany) before freezing in liquid nitrogen and storage at -80 °C[52].

ThS Staining

Inhibition experiment was accomplished by incubation of Aβ1-40 monomers (50 μM) with AuP nanorods (0.3 nM) in CSF at 37 °C for 7 days. For disaggregation experiment, after Aβ1-40 fibrils formed in CSF, AuP (0.3 nM) was added. The mixture was incubated at 37 °C for 20 minutes. Afterward, the mixture was irradiated using an 808 nm NIR laser (1W/cm^2) for 8 minutes. Before measurement, Aβ1-40 samples were diluted with CFS to 10 μM. Then the mixtures were incubated with 20 μM ThS for 20 min. ThS-positive plaques were visualized using an Olympus BX-51 optical system microscope (Tokyo, Japan) at 200 × magnification. Pictures were taken with an Olympus digital camera.

The BBB permeability

S4880202 normal mice were chosen as test animals, in a weight range of 20-25 g (8-12 weeks old) and random in sex. Animals were killed 6h after intravenous injection of 100 μL AuP nanorods (120 μg mL^{-1}, the concentration of Au) in the lateral tail vein. The mouse that treated without AuP was used as the control group. The brain was collected immediately, washed twice with normal saline solution, and dried under vacuum for 48 h at 80 °C. The dried samples were ground into powder, and the powders were acid-digested in 12 M aqua regia overnight. Finally the sample was diluted in 8mL water. The Au content of the samples was measured by ICP-MS (Varian 720-ES). The data points shown were the mean values ± SEM from three independent experiments.

Results and discussion

AuP fabrication

AuNRs with CTAB coating were synthesized using the seed-less growth method[17]. Amino-functionalized AuNRs (AuNR-NH_2) were prepared by covalently grafting 2-aminoethanethiol onto the surface of AuNRs to remove the CTAB. CTAB is a well-known toxic cationic surfactant. Replacing CTAB from the system can dramatically decrease the cytotoxicity of the materials to enhance their biocompatibility in biological application.[53,54] Then, 2-aminoethanethiol coated nanorods could bind with POMs and Aβ15-20 in sequence by an electrostatic interaction. Both energy-dispersive X-ray spectroscopy (EDS) and X-ray photoelectron spectroscopy (XPS) confirmed 2-aminoethanethiol have been successfully conjugated on the surface of the Au nanorods (Figure S1). The TEM image (Figure S2A) depicted the AuNR-NH_2 with an aspect ratio of approximately 3.8 (length: 33 nm, width: 8.6 nm). Owing to the presence of 2-aminoethanethiol, the surface charge of the nanorods revealed a zeta potential of 17.5 mV. Loading POM could reverse the surface charge of AuNRs to negative charged (-26.0 mV) (Table S1). The relatively uniform coating on the surface of AuNRs in Figure S2C indicated that Aβ15-20 was successfully conjugated with Au-POM. The AuNR-NH_2 exhibited a week transverse plasmon band at 520 nm and a strong longitudinal plasmon band at 720 nm. Aβ15-20 attachment could make a slight shift in the characteristic absorbance spectrum of the nanorods, reflecting a change in the local dielectric field resulting from the presence of Aβ15-20 (Figure S3).

Aβ aggregates detection

Once fabricated, firstly we employed the AuP as a bioprobe for monitoring Aβ aggregation. Herein, Aβ1-40 was chosen as the protein model. Aβ1-40, the most common isoform of Aβ, has been widely used for in vitro studies, in which its peculiar effects on neurons have been well illustrated[8]. Upon targeted with Aβ1-40, the Aβ1-40 aggregation can be visualized via Aβ1-40 aggregates induced AuP precipitation (Figure 2A). Addition of Aβ1-40 monomers with the random coil conformations into the solution of AuP made the Aβ1-40 coat on the surface of AuP which could not induce the AuP aggregation (Figure S4). However, in the presence of Aβ1-40 assemblies, the deposits of Aβ1-40 could serve as the template to cause the formation of a network between Aβ15-20-coated nanorods located close together. As shown in Figure 2B, when Aβ1-40 fibrils occurred, the longitudinal plasmon peak of AuP was blue shifted, while the transverse plasmon peak was red-shifted. This typical change of absorption spectra has been assigned to AuP aggregation[35-37]. And the aggregation of AuP was intensified with an increase in the amount of Aβ1-40 fibrils. Moreover, the color of the samples changed from brown to violet with the aggregation of AuP (Figure S5) while the AuP itself showed no changes (Figure S6), indicating that Aβ1-40 fibrils could be even discriminated by naked eyes in our system. The assembly of AuP in the presence of Aβ1-40 fibrils was also confirmed by TEM (Figure S7).

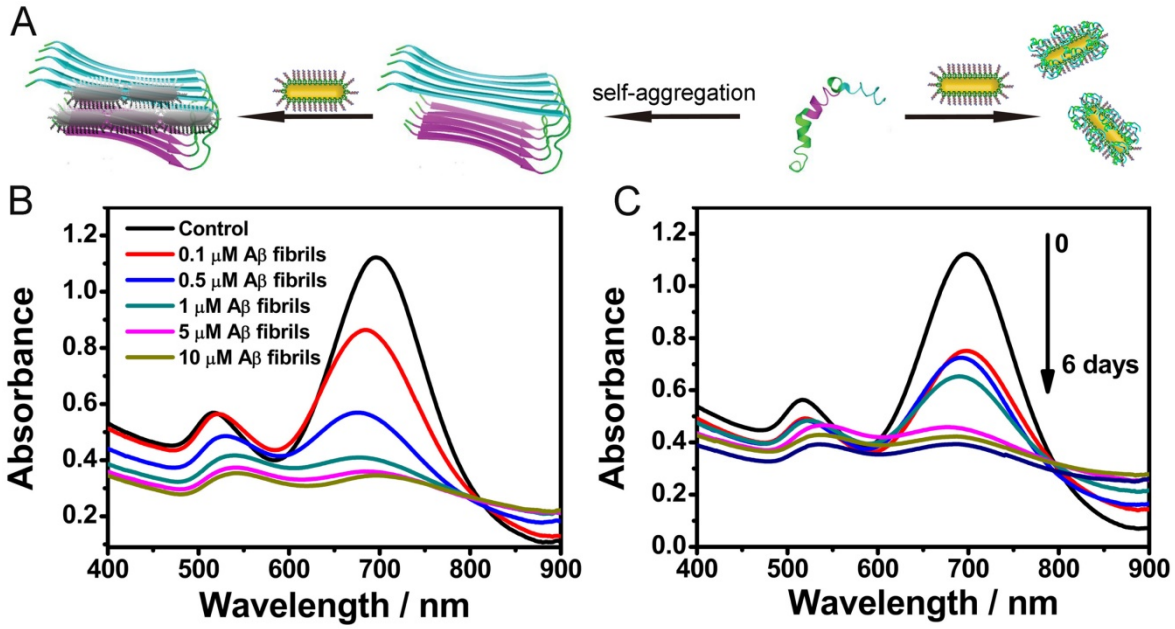

Figure 2. Influence of Aβ1-40 aggregates on the absorption spectra of AuNR. (A) Schematic representation of AuP nanorods used for monitoring Aβ1-40 aggregation. (B) Absorption spectra of AuP in the presence of different concentrations of Aβ1-40 fibrils. The final concentration of AuP nanorods was 0.3 nM. (C) Aβ1-40 fibrillogenesis process monitored by the absorption spectra of AuP nanorods. The final concentration of Aβ1-40 and AuP nanorods were 5 μM and 0.3 nM.

The distinct absorbance behaviors of AuP in the presence of native and fibrillar forms of Aβ1-40 inspired us to explore the possibility of utilizing it to monitor the kinetic process of amyloid fibrosis *ex situ*. After pre-incubation of Aβ1-40 for different days, AuP was added to the resultant solution prior to UV-Vis measurement. As depicted in Figure 2C, the absorbance changed gradually following the increase of incubation time, indicating that aggregation of AuP was enhanced with an increase in the amount of Aβ1-40 aggregates.

Inhibition tests

Having successfully established the ability of AuP for sensing Aβ1-40 aggregates, we next investigated the inhibition activity of these novel nanorods in Aβ1-40 aggregate formation (Figure 3A). To verify the effect of AuP on the assembly of Aβ1-40 into amyloid fibrils, we used a widely used thioflavin T (ThT) fluorescence assay[55-57]. Aβ1-40 was incubated for 7 days in the absence or presence of AuP. When fresh Aβ1-40 alone incubated at 37 °C, ThT fluorescence as a function of incubation time showed a sigmoidal shape (Figure 3B). This result was consistent with the nucleation-dependent polymerization model. However, in the presence of AuP, ThT fluorescence did not increase, which indicated that Aβ1-40 amyloid formation was suppressed. In the control experiment, the nanorods themselves showed no influence on the fluorescence of ThT (Figure S8).

We also performed the effect of the AuP on the morphology of Aβ1-40 aggregates by atomic force microscopy (AFM)[56,57]. As shown in Figure 3C, classical amyloid fibrils were observed in samples of untreated Aβ1-40. The Aβ1-40 fibrils were non-branched, helical filaments with diameters of ~10 nm and lengths of up to several microns. When incubated with AuP nanorods, only small and relatively amorphous aggregates were observed, demonstrating the excellent efficacy of AuP to inhibit Aβ1-40 aggregation (Figure 3D). These results further supported the above results and indicated that AuP nanorods were effective inhibitors for Aβ1-40 aggregation.

It has been proposed that owing to the strong NIR optical absorption ability of AuNRs, the drug which conjugated on the AuNRs via noncovalent interaction can be controllably released from the surface of AuNRs with NIR laser irradiation[58]. To verify the potential of using AuP in photothermal therapy, the AuP solution was exposed to an 808 nm NIR laser with water as the control. In marked contrast to the water sample, the AuP solution showed a rapid increase of temperature when exposed to the laser within a short time (Figure S9). In order to check whether the laser irradiation could make the release of POMs and Aβ15-20 in our system, we used ICP-MS to monitor the release of POM from the AuP. As shown in Figure S10, the amount of POM released about 43.1% after irradiation for 8 min. This release was dependent on irradiation time. The release of Aβ15-20 was confirmed by MALDI-TOF Mass Spectrometry (Figure S11). The released POMs

and Aβ15-20 could enhance the inhibition effect of the AuP for Aβ1-40 aggregation, which was evaluated both by ThT assay and AFM (Figure 3B and Figure 3E). The light-triggered, remotely controlled release of the two inhibitors, POMs and Aβ15-20, from the plasmonic nanorod-based complex presented significant importance for in vivo application in AD treatment.

Disaggregation tests

According to our previous report[33], Aβ1-40 fibrils could be dissociated by local heat. Inspired by the ability of AuNRs to generate local heat, we then monitored the disaggregation effect of AuP on Aβ1-40 aggregates upon NIR irradiation. Aβ1-40 fibrils in aggregation buffer (10 mM Tris, 150 mM NaCl, pH 7.3) were incubated with AuP for 20 min at 37 °C to maximize the targeting effect of Aβ15-20 and Aβ1-40 fibrils. The presence of Aβ1-40 fibrils enhanced the fluorescence of ThT. However, after we exposed the solution to a laser with a power density of 1 Wcm^{-2} to irradiate the AuP-Aβ1-40 aggregates for 8 min, the fluorescence signal of ThT decreased significantly compared with AuP-Aβ1-40 in buffer (Figure S12). In marked contrast, for the irradiation of Aβ1-40 fibrils alone or the AuP with Aβ1-40 aggregates without laser irradiation, the fluorescent signals remained almost unchanged, demonstrating that neither the NIR laser irradiation alone nor AuP by itself can affect the Aβ1-40 structure under our experimental condition. Interestingly, we also performed the same experiment using AuNR-NH_2. As showed in Figure S13, AuNR-NH_2 could also dissociate Aβ1-40 aggregates upon NIR irradiation but less effectively than AuP, indicating the targeting effect of Aβ15-20 on the surface of AuP nanorods was significantly important to the disaggregation ability of AuP upon NIR irradiation. The same results were also observed by using AFM. When incubated with AuP nanorods, the performed Aβ1-40 fibrils remained unchanged, illustrating that AuP nanorods could hardly alter the assembly of Aβ1-40 in a short time (Figure 4B). Interestingly, the Aβ1-40 fibrils induced AuP self-assemble was also easily observed in AFM images (Figure 4D). However, after irradiation with NIR laser, numerous small, relatively amorphous aggregates were observed in the AuP nanorods treated Aβ1-40 samples, demonstrating the excellent efficacy of AuP to disaggregate the amyloid deposits upon NIR laser irradiation (Figure 4C). In addition to the results of Aβ1-40, Aβ1-42 which was more central to neuronal degeneration observed in AD was employed to detect the disaggregation effect of AuP upon NIR irradiation. The similar result was observed (Figure S14).

Inhibition and disaggregation tests in complex matrix

It is well known that Aβ concentrated in CSF is a diagnostic and therapeutic target for AD[59,60]. Therefore, it is important to check whether the functionalized AuP nanorods can effectively inhibit Aβ1-40 aggregation and dissociate Aβ1-40 fibrils in a biological matrix.

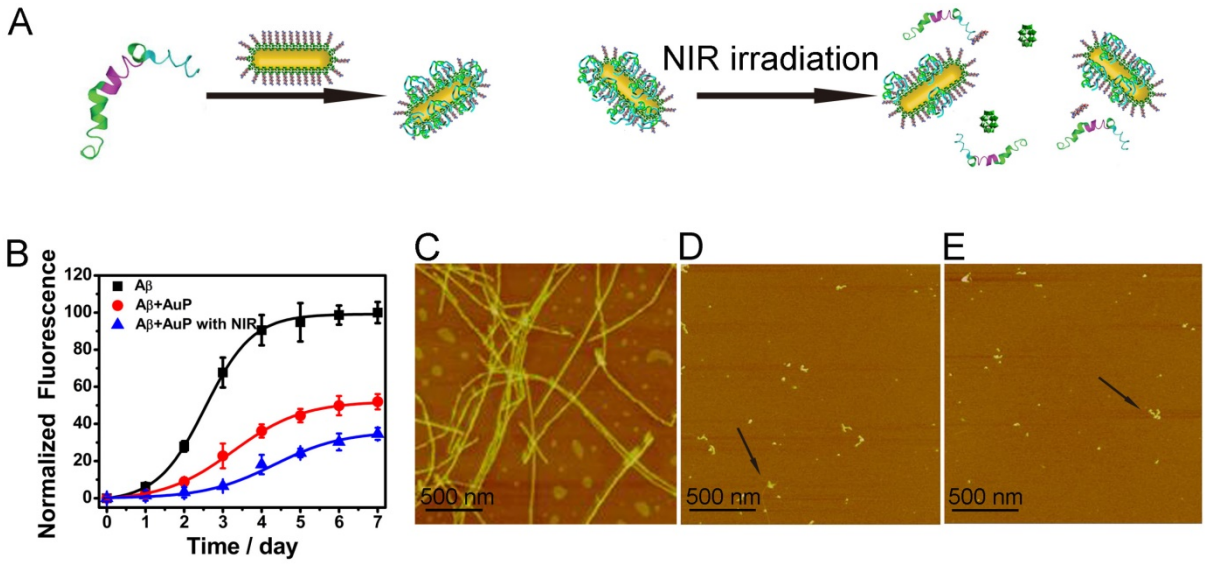

Figure 3. Inhibition of Aβ1-40 aggregation by AuP nanorods. (A) Schematic representation of AuP nanorods used for inhibiting Aβ1-40 aggregation. (B) Fibrillation kinetics of Aβ1-40 as monitored by the development of thioflavin T binding in the absence of AuP nanorods (■) or in the presence of AuP nanorods without NIR (●), or with NIR (▼). (C) AFM image of a control sample containing Aβ1-40 after incubation at 37 °C for 7 days. (D) AFM image of a sample containing Aβ1-40 and AuP nanorods after incubation at 37 °C for 7 days. (E) AFM image of a sample containing Aβ1-40 and AuP nanorods pre-treated with NIR irradiation after incubation at 37 °C for 7 days. The concentration of Aβ1-40 and AuP nanorods were 50 μM and 0.3 nM. Buffer: 10 mM Tris, 150 mM NaCl, pH 7.3. The arrows in Figure D and Figure E indicated the presence of AuP.

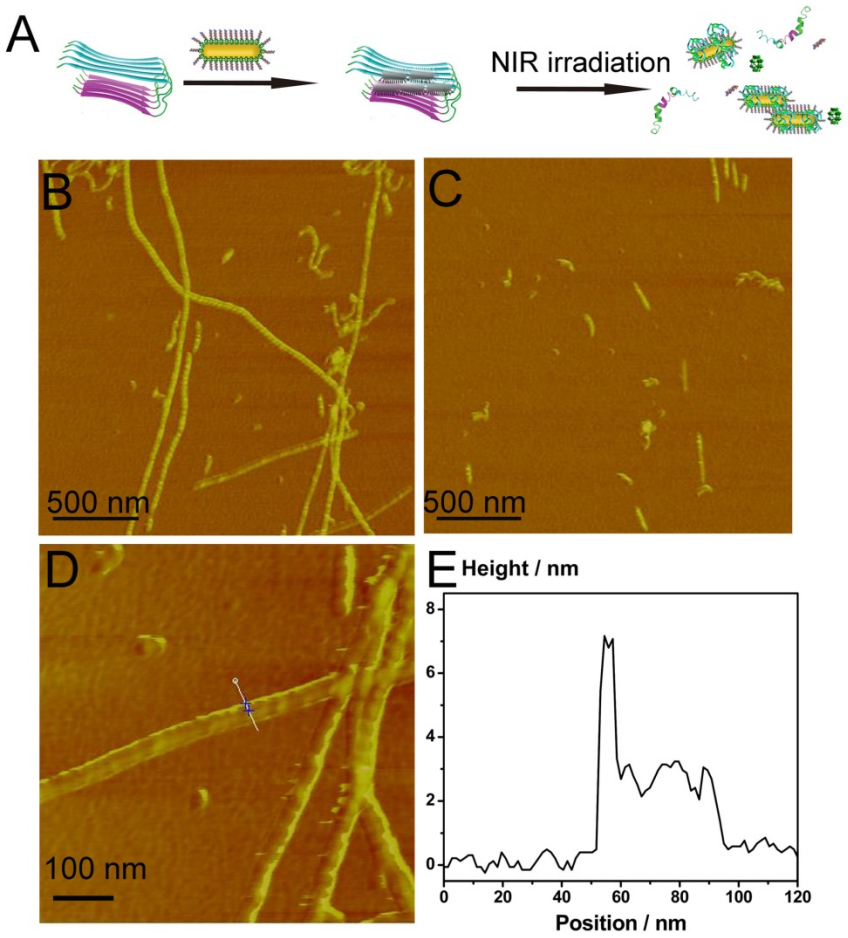

Figure 4. The influence of the photothermal effect of AuP nanorods on Aβ1-40 disaggregation. (A) Schematic representation of AuP nanorods used for dissociating Aβ1-40 aggregation. (B) The morphology of Aβ1-40 fibrils in the presence of AuP nanorods. (C) The morphology of Aβ1-40 fibrils in the presence of AuP under laser irradiation. (D) Locally amplified AFM image in Figure 4B. (E) The height of AuP nanorods aggregated with Aβ1-40 fibrils. The concentration of Aβ1-40 and AuP nanorods were 50 μM and 0.3 nM.

To address this question, we used thioflavin-S (ThS) to stain the Aβ deposit. ThS is a standard fluorescent stain that specifically binds to amyloid protein deposits, leading to emit yellow fluorescence under ultraviolet light[61-64]. As depicted in Figure 5 and Figure S15, Aβ1-40 incubated in CSF for 7 days demonstrated intense birefringence under fluorescence microscopy, indicating the formation of amyloid fibrils. While after treated Aβ1-40 samples with AuP under the same conditions, the fraction of ThS positive deposits decreased, confirming that AuP can inhibit amyloid peptide aggregation. Critically, before co-incubating AuP with Aβ1-40, irradiating the AuP nanorods for 8 min with NIR laser can enhance their inhibition effect on Aβ1-40 aggregation (Figure 5C and Figure S15C). Furthermore, addition of AuP to the performed Aβ1-40 fibrils in CSF could not change the fluorescence of ThS (Figure 5D). However, after exposed the sample to a NIR laser to irradiate the AuP-Aβ1-40 aggregates, the size and abundance of ThS-positive structures was reduced (Figure 5E). These results demonstrated that our synthetic AuP nanorods could successfully produce a marked effect even in complex cerebrospinal fluid.

Cell cytotoxicity tests

Since AuP nanorods can inhibit Aβ1-40 aggregation and dissociate the amyloid deposits and aggregates upon laser irradiation, next we checked whether the nanoparticles can block Aβ1-40-mediated cellular toxicity. The rat pheochromocytoma cell line (PC12), a common model for neuronal functional studies, was used to perform 3-(4,5-dimethylthiazol-2-yl)-2,5-diphenyltetrazolium bromide (MTT) assay to probe cellular metabolism[49,56,57,65,66]. Figure 6A showed that Aβ1-40 fibrils (5 μM) led to a decrease of 46% in cellular reduction of MTT (lane 2). However, treatment of the cells with Aβ1-40 which was co-incubated with AuP for 7 days can significantly increase the cell viability (Figure 6A). And the protection effect of AuP on cells from apoptotic death was enhanced by pretreating the AuP nanorods with NIR irradiation (Figure 6A).

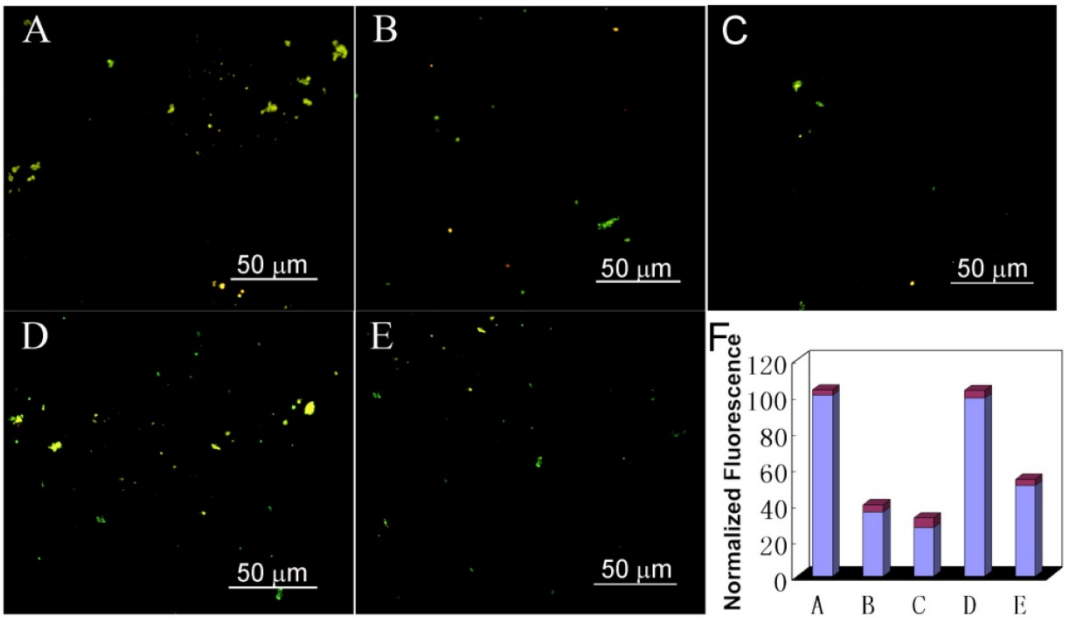

Figure 5. Fluorescence images of Aβ1-40 incubated with AuP nanorods in mice CSF. (A) Aβ1-40 after incubation for 7 days; (B) Aβ1-40 co-incubated with AuP nanorods at 37 °C for 7 days; (C) Aβ1-40 with AuP nanorods pre-treated with NIR irradiation after co-incubation for 7 days; (D) Aβ1-40 fibrils in the presence of AuP nanorods; (E) Aβ1-40 fibrils in the presence of AuP under laser irradiation; (F) The fluorescence of samples from A, B, C, D, E. The concentration of Aβ1-40 and AuP nanorods were 50 μM and 0.3 nM.

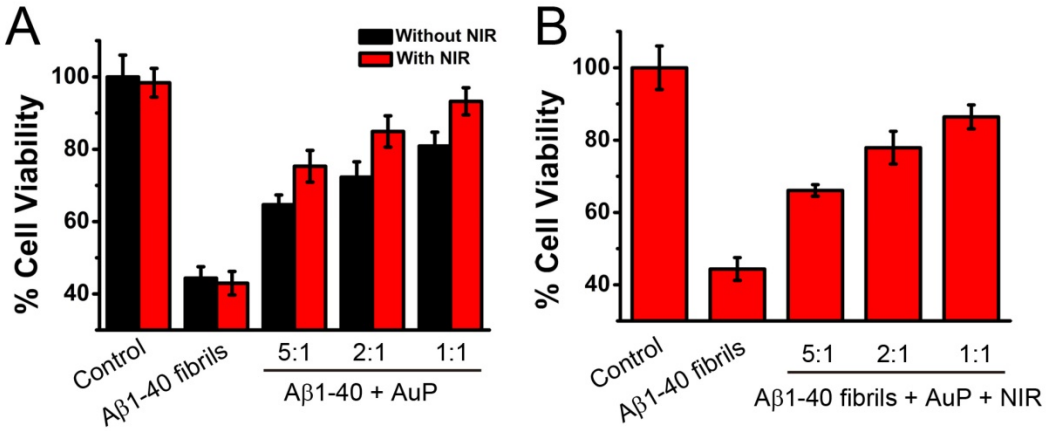

Figure 6. (A) Concentration dependent inhibition effects of AuP nanorods with or without NIR treatment on Aβ1-40-induced cytotoxicity of PC12 cells. (B) AuP nanorods decrease insoluble Aβ40 aggregates-induced cytotoxicity of PC12 cells in a concentration dependent manner upon NIR irradiation. Cell viability was determined using the MTT method and data points shown are the mean values ± standard error of the mean (SEM) from three independent experiments. Control: Aβ1-40 untreated cells. The concentration of Aβ40 was 5 μM. The concentrations of AuP nanorods were 0.03 nM, 0.08 nM and 0.16 nM for the ratio of 5:1, 2:1 and 1:1 (the ratios between Aβ40 and Aβ15-20) respectively.

On the other hand, even after the Aβ1-40 performed, treatment of the cells with Aβ1-40 in the presence of AuP under NIR laser irradiation for 5 minutes could effectively decrease the cytotoxicity of Aβ1-40 (Figure 6B). Furthermore, AuP can prevent Aβ1-40-induced cell death in a dose dependent manner (Figure 6). Aβ1-40 fibrils treated with AuP in the absence of NIR laser irradiation or Aβ1-40 untreated with AuP under NIR laser irradiation, however, did not increase the cell viability (Figure 6). As depicted in Figure S16, AuP themselves and NIR irradiation were non-toxic under the same conditions. As expected, the above results showed that AuP was effective to inhibit Aβ1-40 aggregation and dissolve the existing fibrils of Aβ1-40 evidenced by AFM and spectral analysis and demonstrated in PC12 cells.

BBB permeability

As a suitable candidate for AD treatment, the multifunctional nanorod should have the potential ability to cross BBB. To determine whether AuP can passively accumulate in the brain of living animals, we used ICP-MS to measure the amount of AuP in the brain after intravenous injection for 6 hours. A significant level of Au was found at the brain in the mouse that treated with AuP compared to the control

mouse. The efficiency of AuP accumulation in the brain was about 2.097±0.337% (Table S2), indicating AuP may possess the possible ability to cross BBB. Previous reports demonstrated that near-infrared light (~650-900 nm) with a deep penetration in tissues up to 4-10 cm can be used for in vivo therapy of tumors under skin and deeply seated within tissue even the brain tumors.[67,68,69] These findings shed lights on the potential of AuP nanorods as therapeutic agents to be used in AD treatment. Although promising, a thorough examination of how the nanorods affect tissue organs especially the brain after irradiation treatment would be important and merits further investigation in future studies.

Conclusion

In summary, a new functionalized AuP has been synthesized for not only detection of the Aβ aggregation but also chemotherapeutical and photothermal treatment of AD. Our design combines the unique high NIR absorption property of AuNRs with two known Aβ inhibitors, Aβ15-20 and POM. The synthesized AuP can effectively inhibit Aβ aggregation and dissociate amyloid deposits with NIR irradiation both in buffer and in mice CSF, and protect cells from Aβ-related toxicity upon NIR irradiation. Compared with traditional drug strategies, the functional AuP possesses the potential ability to cross the BBB which overcomes the drawbacks of unstable β-sheet breaker peptides. Furthermore, the hyperthermic effects of AuP have been considered important and useful in clinical treatment with reduced side effects. In addition, the process of Aβ aggregation can be monitored by the absorbance change of AuNRs. The AuNRs act as not only diagnostic probes but also drug carriers and photothermal reagents in our work. So far, there is no report to integrate three segments: an Aβ-targeting element, a reporter and inhibitors in one system for AD treatment. Our results could provide new insights into the design of new multifunctional nanomaterial for both sensitive detection of AD pathology and effective treatment of AD.

Acknowledgements

The authors thank Prof. Enbo Wang for providing the POMs. We acknowledge financial support from 973 Project (2012CB720602), and NSFC (21210002, 21431007, 21533008).

Supplementary Material

Figure S1 - Figure S14.
http://www.thno.org/v07p2996s1.pdf

Competing Interests

The authors have declared that no competing interest exists.

References

1. Soto C. Unfolding the role of protein misfolding in neurodegenerative diseases. Nat Rev Neurosci. 2003; 4: 49-60.
2. Barnham KJ, Masters CL, Bush AI. Neurodegenerative diseases and oxidative stress. Nat Rev Drug Discov. 2004; 3: 205-14.
3. Hamley IW. The amyloid beta peptide: a chemist's perspective. Role in Alzheimer's and fibrillization. Chem Rev. 2012; 112: 5147-92.
4. Scott LE, Orvig C. Medicinal inorganic chemistry approaches to passivation and removal of aberrant metal ions in disease. Chem Rev. 2009; 109: 4885-910.
5. Gaggelli E, Kozlowski H, Valensin D, Valensin G. Copper homeostasis and neurodegenerative disorders (Alzheimer's, prion, and Parkinson's diseases and amyotrophic lateral sclerosis). Chem Rev. 2006; 106: 1995-2044.
6. Ghiam Y, Kenjiro O, Mohammed I. Amyloid β-protein assembly as a therapeutic target of Alzheimer's disease. Curr Pharm Des. 2008; 14: 3231-46.
7. Taylor M, Moore S, Mayes J, et al. Development of a proteolytically stable retro-inverso peptide inhibitor of β-amyloid oligomerization as a potential novel treatment for Alzheimer's disease. Biochemistry. 2010; 49: 3261-72.
8. Hyung SJ, DeToma AS, Brender JR, et al. Insights into antiamyloidogenic properties of the green tea extract (-)-epigallocatechin-3-gallate toward metal-associated amyloid-β species. Proc Natl Acad Sci USA. 2013; 110: 3743-8.
9. Yang W, Wong Y, Ng OT, et al. Inhibition of Beta-Amyloid Peptide Aggregation by Multifunctional Carbazole-Based Fluorophores. Angew Chem Int Ed. 2012; 51: 1804-10.
10. Takahashi T, Mihara H. Peptide and protein mimetics inhibiting amyloid β-peptide aggregation. Acc Chem Res. 2008; 41: 1309-18.
11. Frydman-Marom A, Rechter M, Shefler I, Bram Y, Shalev DE, Gazit E. Cognitive-performance recovery of Alzheimer's disease model mice by modulation of early soluble amyloidal assemblies. Angew Chem Int Ed. 2009; 48: 1981-6.
12. Tjernberg LO, Naslund J, Lindqvist F, Johansson J, Karlstromi AR, Thyberg J. Arrest of beta-amyloid fibril formation by a pentapeptide ligand. J Biol Chem. 1996; 271: 8545-8.
13. Liu L, Xu K, Wang H, et al. Self-assembled cationic peptide nanoparticles as an efficient antimicrobial agent. Nat Nanotechnol. 2009; 4: 457-63.
14. Pan H, Soman NR, Schlesinger PH, Lanza GM, Wickline SA. Cytolytic peptide nanoparticles ('NanoBees') for cancer therapy. Nanomed Nanobiotechnol. 2011; 3: 318-27.
15. Li M, Xu C, Wu L, Ren J, Wang E, Qu X. Self-Assembled Peptide–Polyoxometalate Hybrid Nanospheres: Two in One Enhances Targeted Inhibition of Amyloid β-Peptide Aggregation Associated with Alzheimer's Disease. Small. 2013; 9: 3455-61.
16. Geng J, Li M, Wu L, Chen C, Qu X. Mesoporous Silica Nanoparticle-based H_2O_2 Responsive Controlled-Release System Used for Alzheimer's Disease Treatment. Adv Healthcare Mater. 2012; 1: 332-6.
17. Yang X, Liu X, Liu Z, Pu F, Ren J, Qu X. Near-Infrared Light-Triggered, Targeted Drug Delivery to Cancer Cells by Aptamer Gated Nanovehicles. Adv Mater. 2012; 24: 2890-5.
18. Li M, Shi P, Xu C, Ren J, Qu X. Cerium oxide caged metal chelator: anti-aggregation and anti-oxidation integrated H_2O_2-responsive controlled drug release for potential Alzheimer's disease treatment. Chem Sci. 2013; 4: 2536-42.
19. Feng X, Lv F, Liu L, Yang Q, Wang S, Bazan GC. A highly emissive conjugated polyelectrolyte vector for gene delivery and transfection. Adv Mater. 2012; 24: 5428-32.
20. Wiley DT, Webster P, Gale A, Davis ME. Transcytosis and brain uptake of transferrin-containing nanoparticles by tuning avidity to transferrin receptor. Proc Natl Acad Sci USA. 2013; 110: 8662-7.
21. Ren J, Shen S, Wang D, et al. The targeted delivery of anticancer drugs to brain glioma by PEGylated oxidized multi-walled carbon nanotubes modified with angiopep-2. Biomaterials. 2012; 33: 3324-33.
22. Nie G, Hah HJ, Kim G, et al. Hydrogel nanoparticles with covalently linked coomassie blue for brain tumor delineation visible to the surgeon. Small. 2012; 8: 884-91.
23. Wohlfart S, Gelperina S, Kreuter J. Transport of drugs across the blood-brain barrier by nanoparticles. J Control Release. 2012; 161: 264-73.
24. Dilnawaz F, Singh A, Mewar S, Sharma U, Jagannathan NR, Sahoo SK. The transport of non-surfactant based paclitaxel loaded magnetic nanoparticles across the blood brain barrier in a rat model. Biomaterials. 2012; 33: 2936-51.
25. Ni W, Kou X, Yang Z, Wang J. Tailoring longitudinal surface plasmon wavelengths, scattering and absorption cross sections of gold nanorods. ACS Nano. 2008; 2: 677-86.
26. Eghtedari M, Oraevsky A, Copland JA, Kotov NA, Conjusteau A, Motamedi M. High sensitivity of in vivo detection of gold nanorods using a laser optoacoustic imaging system. Nano Lett. 2007; 7: 1914-8.
27. Chen CC, Lin YP, Wang CW, et al. DNA-gold nanorod conjugates for remote control of localized gene expression by near infrared irradiation. J Am Chem Soc. 2006; 128: 3709-15.

28. Huang X, El-Sayed IH, Qian W, El-Sayed MA. Cancer cell imaging and photothermal therapy in the near-infrared region by using gold nanorods. J Am Chem Soc. 2006; 128: 2115-20.
29. Huang J, Jackson KS, Murphy CJ. Polyelectrolyte wrapping layers control rates of photothermal molecular release from gold nanorods. Nano Lett. 2012; 12: 2982-7.
30. Kuo TR, Hovhannisyan VA, Chao YC, et al. Multiple release kinetics of targeted drug from gold nanorod embedded polyelectrolyte conjugates induced by near-infrared laser irradiation. J Am Chem Soc. 2010; 132: 14163-71.
31. Kogan MJ, Bastus NG, Amigo R, et al. Nanoparticle-mediated local and remote manipulation of protein aggregation. Nano Lett. 2006; 6: 110-5.
32. Adura C, Guerrero S, Salas E, et al. Stable conjugates of peptides with gold nanorods for biomedical applications with reduced effects on cell viability. ACS Appl Mater Interfaces. 2013; 5: 4076-85.
33. Li M, Yang X, Ren J, Qu K, Qu X. Using Graphene Oxide High Near-Infrared Absorbance for Photothermal Treatment of Alzheimer's Disease. Adv Mater. 2012; 24: 1722-8.
34. Xiao Q, Zheng X, Bu W, et al. A Core/Satellite Multifunctional Nanotheranostic for in Vivo Imaging and Tumor Eradication by Radiation/Photothermal Synergistic Therapy. J Am Chem Soc. 2013; 135: 13041-8.
35. Yu C, Irudayaraj J. Multiplex biosensor using gold nanorods. Anal Chem. 2007; 79: 572-9.
36. Caswell KK, Wilson JN, Bunz UHF, Murphy CJ. Preferential end-to-end assembly of gold nanorods by biotin-streptavidin connectors. J Am Chem Soc. 2003; 125: 13914-5.
37. Park HS, Agarwal A, Kotov NA, Lavrentovich OD. Controllable side-by-side and end-to-end assembly of Au nanorods by lyotropic chromonic materials. Langmuir. 2008; 24: 13833-7.
38. Singh AK, Senapati D, Wang S, et al. Gold nanorod based selective identification of Escherichia coli bacteria using two-photon Rayleigh scattering spectroscopy. ACS Nano. 2009; 3: 1906-12.
39. Kida T. Synthesis of gold nanosheets at a liquid/liquid interface using an amphiphilic polyoxometallate/surfactant hybrid photocatalyst. Langmuir. 2008; 24: 7648-50.
40. Kang Z, Wang E, Jiang M, Lian S. Synthesis and characterization of polyoxometalate nanowires based on a novel microemulsion process. Nanotechnology. 2004; 15: 55-8.
41. Carraro M, Sartorel A, Scorrano G, et al. Chiral Strandberg-Type Molybdates $[(RPO_3)_2Mo_5O_{15}]^{2-}$ as Molecular Gelators: Self-Assembled Fibrillar Nanostructures with Enhanced Optical Activity. Angew Chem Int Ed. 2008; 47: 7275-9.
42. Liu S, Kurth DG, Bredenkötter B, Volkmer D. The Structure of Self-Assembled Multilayers with Polyoxometalate Nanoclusters. J Am Chem Soc. 2002; 124: 12279-87.
43. Nisar A, Zhuang J, Wang X. Cluster-based self-assembly: Reversible formation of polyoxometalate nanocones and nanotubes. Chem Mater. 2009; 21: 3745-51.
44. Zhang J, Song YF, Cronin L, Liu T. Self-Assembly of Organic-Inorganic Hybrid Amphiphilic Surfactants with Large Polyoxometalates as Polar Head Groups. J Am Chem Soc. 2008; 130: 14408-9.
45. Li H, Sun H, Qi W, Xu M, Wu L. Onionlike Hybrid Assemblies Based on Surfactant-Encapsulated Polyoxometalates. Angew Chem Int Ed. 2007; 46: 1300-3.
46. Ritchie C, Cooper GJ, Song YF, et al. Spontaneous assembly and real-time growth of micrometre-scale tubular structures from polyoxometalate-based inorganic solids. Nat Chem. 2009; 1: 47-52.
47. Zhang C, Bu W, Ni D, et al. A Polyoxometalate Cluster Paradigm with Self-Adaptive Electronic Structure for Acidity/Reducibility-Specific Photothermal Conversion. J Am Chem Soc. 2016; 138: 8156-64.
48. Shaw CP, Middleton DA, Volk M, Lévy R. Amyloid-derived peptide forms self-assembled monolayers on gold nanoparticle with a curvature-dependent β-sheet structure. ACS Nano. 2012; 6: 1416-26.
49. Geng J, Li M, Ren J, Wang E, Qu X. Polyoxometalates as inhibitors of the aggregation of amyloid β peptides associated with Alzheimer's disease. Angew Chem Int Ed. 2011; 50: 4184-8.
50. Schlamadinger DE, Kats DI, Kim JE. Quenching of tryptophan fluorescence in unfolded cytochrome c: A biophysics experiment for physical chemistry students. J Chem Educ. 2010; 87: 961-4.
51. Puchalski MM, Morra MJ, von Wandruszka R. Assessment of inner filter effect corrections in fluorimetry. Fresenius J Anal Chem. 1991; 340: 341-4.
52. Barten DM, Guss VL, Corsa JA, et al. Dynamics of β-amyloid reductions in brain, cerebrospinal fluid, and plasma of β-amyloid precursor protein transgenic mice treated with a γ-secretase inhibitor. J Pharmacol Exp Ther. 2005; 312: 635-43.
53. Murphy CJ, Gole AM, Stone JW, et al. Gold nanoparticles in biology: beyond toxicity to cellular imaging. Acc Chem Res. 2008; 41: 1721-30.
54. Qiu Y, Liu Y, Wang L, et al. Surface chemistry and aspect ratio mediated cellular uptake of Au nanorods. Biomaterials. 2010; 31: 7606-19.
55. LeVine III H. Thioflavine T interaction with synthetic Alzheimer's disease β-amyloid peptides: Detection of amyloid aggregation in solution. Protein Sci. 1993; 2: 404-10.
56. Yu H, Li M, Liu G, et al. Metallosupramolecular complex targeting an α/β discordant stretch of amyloid β peptide. Chem Sci. 2012; 3: 3145-53.
57. Geng J, Li M, Wu L, Ren J, Qu X. Liberation of copper from amyloid plaques: making a risk factor useful for Alzheimer's disease treatment. J Med Chem. 2012; 55: 9146-55.
58. Wijaya A, Schaffer SB, Pallares IG, Hamad-Schifferli K. Selective release of multiple DNA oligonucleotides from gold nanorods. ACS Nano. 2009; 3: 80-6.
59. Halim A, Brinkmalm G, Rüetschi U, et al. Site-specific characterization of threonine, serine, and tyrosine glycosylations of amyloid precursor protein/amyloid β-peptides in human cerebrospinal fluid. Proc Natl Acad Sci USA. 2011; 108: 11848-53.
60. Blennow K, Hampel H, Weiner M, Zetterberg H. Cerebrospinal fluid and plasma biomarkers in Alzheimer disease. Nat Rev Neurol. 2010; 6: 131-44.
61. Santa-María I, Pérez M, Hernández F, Avila J, Moreno FJ. Characteristics of the binding of thioflavin S to tau paired helical filaments. J Alzheimers Dis. 2006; 9: 279-85.
62. Boshuizen RS, Langeveld JP, Salmona M, Williams A, Meloen RH, Langedijk JP. An in vitro screening assay based on synthetic prion protein peptides for identification of fibril-interfering compounds. Anal Biochem. 2004; 333: 372-80.
63. Urbanc B, Cruz L, Le R, et al. Neurotoxic effects of thioflavin S-positive amyloid deposits in transgenic mice and Alzheimer's disease. Proc Natl Acad Sci USA. 2002; 99: 13990-5.
64. Hu X, Crick SL, Bu G, Frieden C, Pappu RV, Lee JM. Amyloid seeds formed by cellular uptake, concentration, and aggregation of the amyloid-beta peptide. Proc Natl Acad Sci USA. 2009; 106: 20324-9.
65. Peters I, Igbavboa U, Schütt T, et al. The interaction of beta-amyloid protein with cellular membranes stimulates its own production. Biochim Biophys Acta. 2009; 1788: 964-72.
66. Wiessner C, Wiederhold KH, Tissot AC, et al. The second-generation active Aβ immunotherapy CAD106 reduces amyloid accumulation in APP transgenic mice while minimizing potential side effects. J Neurosci. 2011; 31: 9323-31.
67. Tucker-Schwartz JM, Meyer TA, Patil CA, Duvall CL, Skala MC. In vivo photothermal optical coherence tomography of gold nanorod contrast agents. Biomed Opt Express. 2012; 3: 2881-95.
68. Weissleder R. A clearer vision for in vivo imaging. Nat Biotechnol. 2001; 19: 316-7.
69. Schwartz JA, Shetty AM, Price RE, et al. Feasibility study of particle-assisted laser ablation of brain tumors in orthotopic canine model. Cancer Res. 2009; 69: 1659-67.